Nonlinear interaction processes between a CO_2 laser and a plasma

S. Nakai, M. Matoba, H. Fujita, H. Nishimura, H. Daido, N. Banjyoya, K. Iba, and C. Yamanaka
Institute of Laser Engineering, Osaka University, Osaka, Japan
(Received 4 January 1977; revised manuscript received 1 November 1977)

The coupling mechanism of a CO_2 laser with a plasma has been investigated. The parametric decay instability, stimulated Brillouin backscattering, and the modulational instability were observed at theoretically predicted laser power thresholds. The modulational instability seems to be responsible for the generation of magnetic fields and fast ions.

I. INTRODUCTION

The interaction of an intense laser beam with a plasma is one of the most interesting aspects of laser fusion research. This problem has been investigated mainly by using Nd-glass lasers.[1-3] Here we present experimental results on the coupling of a CO_2 laser with a plasma. The longer wavelength of the CO_2 laser lowers the threshold power of the various instabilities which contribute to absorption and reflection. Scaling analysis of Nd-glass and CO_2 laser experiments will give us more detailed information about the interaction mechanisms than can be obtained by experiments at one wavelength.

An E-beam controlled CO_2 laser system[4,5] was used. The laser light of output power up to 20 J in 4 nsec was focused by a Ge lens onto solid or film plastic targets. The maximum power density was about 10^{12} W/cm^2. Various nonlinear processes such as change of reflectivity, generation of fast ions, stimulated Brillouin backscattering, and self-induced magnetic fields were investigated.

II. EXPERIMENTAL ARRANGEMENT

The laser system is composed of an oscillator, three preamplifiers and two main amplifiers. The oscillator and the preamplifiers are uv preionized transversely excited atmosphere (TEA) lasers, the cross section of each is 20×20 mm and the length of each stage is 60 cm. The main amplifiers are E-beam-controlled CO_2 lasers. The cross section of the first stage is 50×50 mm, and the length is 80 cm. The second stage is 100×100 mm in cross section and 100 cm in length. A pulse-shaping system consisting of a laser-triggered spark gap, a GaAs Pockels cell and Ge plate Brewster polarizers is placed between the oscillator and preamplifier. The pulse duration is continuously variable from 2 to 100 nsec with a rise time of 1 nsec. The contrast ratio just after the pulse shaper is better than 1:1000 and degrades to 1:500 after passing through the preamplifiers. The main amplifiers can amplify the power up to 20 J in 4 nsec without any change in the contrast ratio. The output laser light is focused by a Ge lens having a focal length of 100 mm onto solid or film targets. The focal position is determined by measuring the size of the perforated hole on film targets at various distances from the lens. The accuracy of positioning of the target at the focus is better than 100 μm. The focal spot is 400 μm in diameter which corresponds to the size determined by the beam divergence of 4 mrad and the focal length of the lens. The arrangement of the system is shown in Fig. 1. The details of this system and the performance were reported elsewhere.[6]

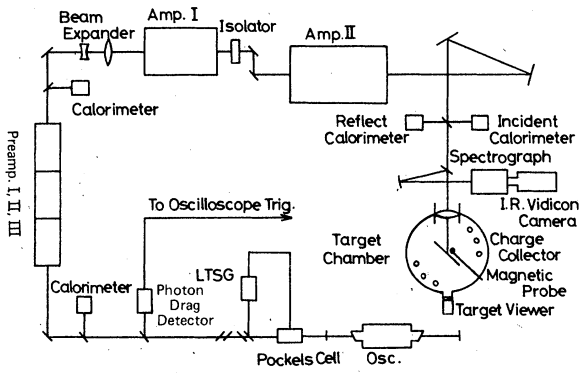

FIG. 1. Schematic diagram of laser and laser plasma experiment.

III. EXPERIMENTAL RESULTS

A. Specular reflectivity and ion collection

The reflectivity of the incident laser light from the laser-produced plasma is measured by the ratio of the output of two calorimeters which are located on opposite sides of a thin film beam splitter as shown in Fig. 1. In the case of a long laser pulse, i.e., 30 nsec, the change of reflectivity at normal incidence on the plane surface of polyethylene targets with increasing laser power density is as shown in Fig. 2. The reflectivity increases to

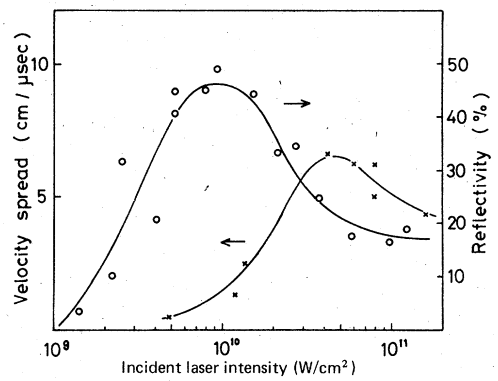

FIG. 2. Change of reflectivity and velocity spread of expanding ions as a function of incident laser intensity.

almost 50% at a power density of 10^{10} W/cm^2 and then decreases to about 18%.

Ion measurements were made with an ion collector located 10 cm from the focal point and at an angle of 50° from the incident-beam axis. Typical oscilloscope traces are shown in Fig. 3 for various incident powers. The time of flight decreases with increasing power, but the rise time increases. This is due to the increase in velocity spread of the blow-off plasma. The velocity spread $\Delta v = (l/t^2)\Delta t$, where l is the flight path, is plotted in Fig. 2. It shows a steep increase at a power level of 10^{10} W/cm^2 which corresponds to the power level of the reflectivity maximum. The velocity spread begins to decrease with the appearance of a prepeak signal at the ion collector as shown in Fig. 3. Below the power level of the prepeak appearance, the energy distribution derived from the velocity spread of the ion collector signal can be fitted to a single Maxwellian distribution which can be clearly distinguished from the energy distribution corresponding to the signal with a prepeak. For a short 4-nsec-wide pulse, the reflectivity above 10^{11} W/cm^2 is almost constant and is about 8%.

To measure the angular distribution of the ejected ions, a thin-film target of Mylar of thickness 3

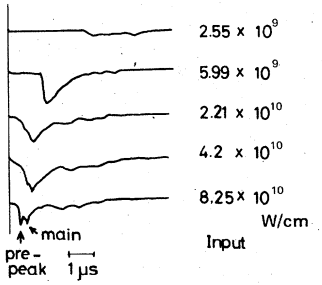

FIG. 3. Signal waveforms of an ion collector. The prepeak increases with larger laser power.

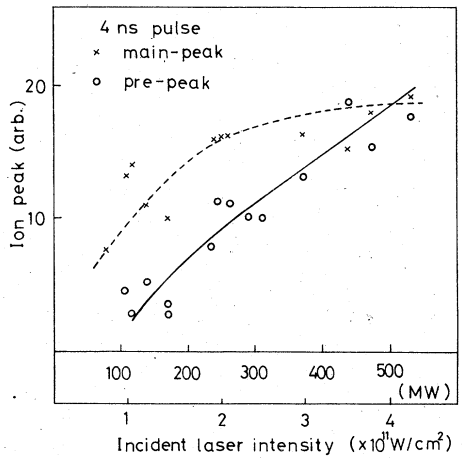

FIG. 4. Relative height of main peak and prepeak as a function of incident laser intensity.

μm is placed with its surface normal at an angle of 50° from the incident laser axis. The prepeak ion signal, which appears at power densities above the level of the reflectivity maximum, is observed within a cone of half-angle 40° about the surface normal in contrast with the isotropic distribution of the main peak. On another collector placed behind the film target only a slow-ion component is observed, and these ions are much slower than the slow component signal from the front collector. As shown in Fig. 4, the amplitude of the ion prepeak at the front collector increases with increasing power density while the main peak saturates. These results show that an anomalous interaction produces the fast-ion component and reduces the reflectivity.

B. Backscattered light and its spectrum

When the target is tilted with its normal at an angle of 50° with respect to the laser beam, the specular back reflection into the focusing cone disappears. By increasing the incident power density, backscattered light is observed above a certain threshold intensity. The points marked by crosses in Fig. 5 are obtained with long laser pulses of 70-nsec width. The points denoted by circles are the results obtained with a 4-nsec-wide short pulse. For long pulses the backscattered power first increases as the square of the incident power, and then saturates. The corresponding reflectivities are also shown. The maximum reflectivity is about 0.6% and then decreases to 0.3%. For short pulses, saturation in reflectivity is not observed within the range of power level so far covered. Threshold power densities for the onset of backscattering can be obtained. They are 2×10^{10} W/cm^2 for the long pulse and 3.6×10^{11} W/cm^2 for

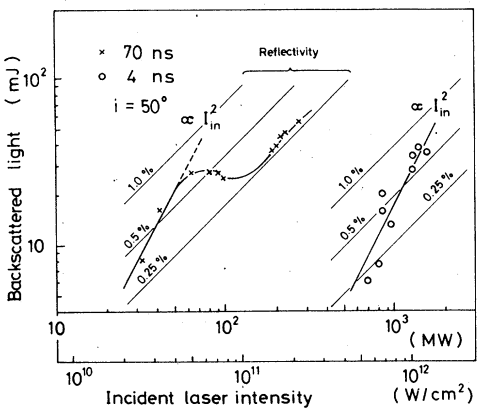

FIG. 5. Back reflection in the case of oblique incidence.

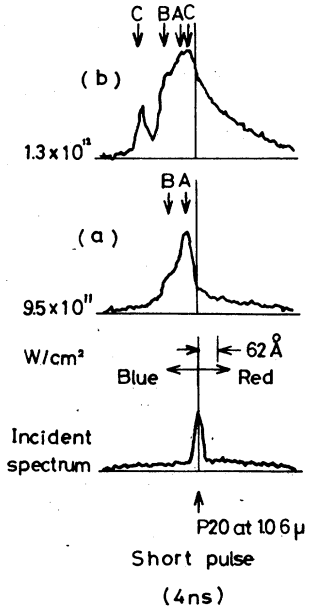

FIG. 6. Spectrum of back-reflected light in the case of oblique incidence. Direction of the shift (red or blue) and calibrated scale of wavelength are shown.

the short pulse. Below these threshold power densities, the backscattered energies decrease abruptly to zero as measured by detectors having a lower detection sensitivity of about 1 mJ. Even below these thresholds for backscattering, the prepeak ion signal is observed and the specular reflectivity is as high as 8% in the case of normal incidence, as mentioned above. Therefore the mechanism of fast-ion generation is apparently different from that responsible for the backscattering.

The spectrum of the backscattered light is measured using an Optical Engineering Model 16-A spectrograph and an ir Vidicon camera having a model TH 9840 pyroelectric image tube of Thomson-CSF. The image at the focal plane of the spectrograph is magnified and focused on the photocathode of the camera tube by a Ge lens. The magnified image on the photocathode is recorded on a video tape recorder and reproduced on an oscilloscope. The overall resolution is 30 Å, which is the full width at half maximum of the incident laser light from the $P(20)$ 10.6-μm CO_2 line.

Typical oscillograph traces of the spectrum are shown in Fig. 6. At power densities lower than 10^{12} W/cm², for short pulses of 4-nsec pulse width, the spectrum of back-reflected light shifts towards the blue as a whole and splits into two peaks as indicated by arrows A and B in trace (a). At power densities above 10^{12} W/cm² another component, C, appears as shown in trace (b). It should be noted that C appears asymmetrically on both sides of peak B. Both C peaks on each side appear simultaneously at the same power density. On the red side, C is superimposed on A and results in a complicated and broadened spectrum. On the blue side, a single peak is clearly observed.

The magnitude of the blue shift of B relative to the incident spectrum corresponds quite well to the Doppler shift due to plasma expansion. The peak A could be due to stimulated Brillouin backscattering (SBS) which shifts towards the red from the Doppler-blue-shifted B. The component C is related to self-phase modulation and will be discussed below.

For long pulses, the general features are similar to those measured for short pulses. Above the power density at which C appears, one component on the red side of A has the appearance of C in trace (b) in Fig. 6 for the short-pulse case, but it has no counterpart on the blue side of B.

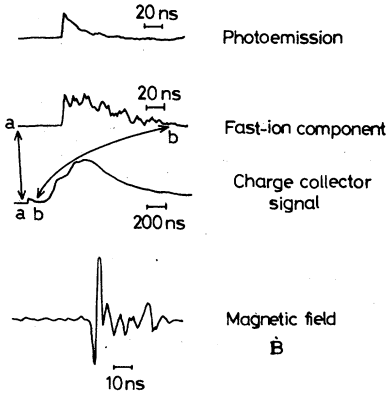

FIG. 7. Charge-collector signal and magnetic-probe signal. The latter is recorded without integrator.

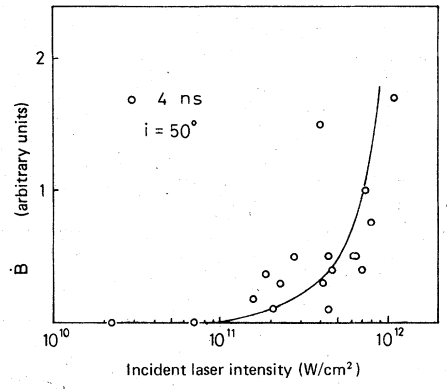

FIG. 8. Growth of $\dot{B}$ peak voltage with increasing incident power.

C. Fast-ion ejection and self-magnetic field

At the power density at which C appears, a self-induced magnetic field is detected by a magnetic probe placed near the focal point. The probe is a four-turn pickup coil having a diameter of 2 mm, which is shielded by thin copper foil and covered by a glass sleeve. The thickness of the foil is thinner than the skin depth of the high frequency corresponding to a pulse with a rise time of 1 nsec. A typical signal is shown in Fig. 7. The peak value of $\dot{B}$ is plotted versus power in Fig. 8. When the $\dot{B}$ peak voltage increases noticeably, superfast ions are ejected normal to the target surface as shown in Fig. 7. At the collector in a direction 20° from the surface normal, no superfast ion component is seen but only the photoemission signal is observed as is shown by the uppermost trace in Fig.

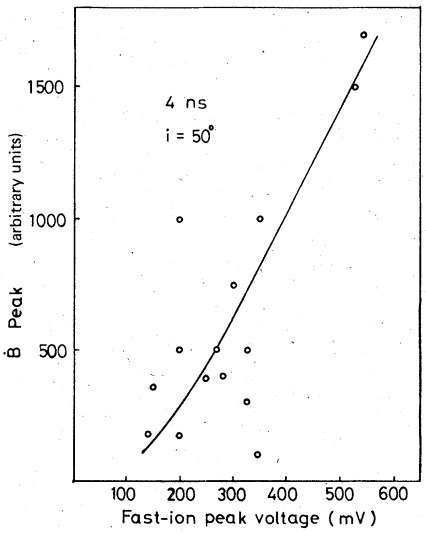

FIG. 9. Correlation of $\dot{B}$ peak voltage and fast-ion peak voltage.

7. When the power density is lower than the threshold value, only the photoemission signal is observed in a direction normal to the target surface. The energies of the fast ions range from about 20 keV up to 50 keV. The correlation between $\dot{B}$ peak voltages and fast-ion peaks on the charge-collector signals is shown in Fig. 9. A definite correlation is observed. The direction of B is the same as it would if it were produced by a current flowing out from the target toward the laser beam. This is consistent with the theoretical model which predicts the generation of collimated fast ions by the existence of magnetic fields.[7]

IV. DISCUSSION

From the experimental results, three distinct features can be noticed corresponding to the three different threshold power densities.

The first is the onset of a decrease of reflectivity accompanied by a steep increase of the velocity spread of the ions and the appearance of an ion-prepeak. This threshold value of 10^{10} W/cm² corresponds to that of the parametric decay instability.[8] The velocity distribution of the expanding plasma begins to deviate from Maxwellian at this laser intensity. Other experiments with TEA lasers have shown a similar behavior in reflectivity[9] and absorption at the same power density.[10]

The second feature is the onset of backscattered light for the case of oblique incidence. The threshold power of $(3-4)\times10^{11}$ W/cm² for a short pulse (Fig. 5) corresponds to the threshold for stimulated Brillouin scattering. The observed spectrum also shows red-shifted scattering (Peak A in Fig. 6, 36–60 Å) relative to the plasma which itself is expanding toward the observer (Doppler-blue-shifted peak B, 60–90 Å), with the measured expansion velocity of $(1-2)\times10^{7}$ cm/sec. The 60-Å red shift corresponds to an acoustic frequency of 1.8×10^{10} Hz and an ion sound speed of 9×10^{6} cm/sec. The threshold power for a long pulse is 2×10^{10} W/cm². For a convective instability such as SBS, the threshold power density is inversely proportional to the scale length of the density gradient. If we assume that the scale length is proportional to the pulse length of laser light, the observed difference in the threshold power densities for the short and long pulses can be explained. The assumption made here is not too unrealistic because the photon pressure at the power density is much less than the expanding plasma pressure and self-similar expansion can be expected. Several SBS measurements using CO_2 lasers have been reported recently from a laser-produced plasma[11] and from underdense plasmas[12,13] with similar red shifts but poor spectral resolution.

The third feature is the appearance of the symmetric side peaks C in the backscattered spectrum which is associated with the generation of self-induced magnetic fields and the generation of collimated superfast ions. The cause of such a spectrum could be explained by the self-phase-modulation of laser light due to density depression.[3] The phase shift $\phi(x,t)$ of a plane wave propagating in the x direction through a medium of instantaneous refractive index $n(x,t)$ is

$$\phi(x,t)=\frac{\omega_0}{C}\int n(x,t)\,dx\ , \tag{1}$$

where ω_0 is the frequency of the incident plane wave, and c is the velocity of light in vacuum. Assuming the refractive index $n(x,t)$ to be constant throughout the density-depressed region D for simplicity, the frequency shift due to the self-phase-modulation can be given by

$$\Delta\omega=-\frac{\partial\phi}{\partial t}=-k_0\left(\frac{\partial n(t)}{\partial t}D+n(t)\frac{\partial D}{\partial t}\right)\ . \tag{2}$$

The first term on the right-hand side corresponds to the phase change due to the refractive-index change caused by the density depression. The second term corresponds to that due to the movement of the critical density surface that is the upper limit of the integration in Eq. (1). If we neglect the second term and use the measured frequency shift $\Delta\omega=2\pi\times2.5\times10^{10}$ rad/sec, the minimum size of the density-depressed region D becomes 250 μm which corresponds to full depression ($\delta N/N_0=1$) near the critical density region during the pulse rise time (1 nsec) of the incident laser light. Here N_0 is the initial electron density $\delta N=N_0-N_e$ and N_e is the depressed electron density.

The density modulation, taking into account the swelling factor, is given by[14]

$$\frac{\delta N}{N_0}\simeq\frac{1}{6\pi^2}\frac{I}{I_{nl}}\Phi^2(\tau)\left(\frac{\lambda_0^3 L}{\lambda_D^4}\right)^{1/3}\ , \tag{3}$$

where I and I_{nl} are the incident laser intensity and the intensity at which the kinetic energy of the electrons oscillating in the laser field becomes comparable to the mean thermal energy of the plasma, respectively, $\Phi(\tau)$ is a resonance function which is given as a function of $\tau=(k_0L)^{1/3}\sin\theta$,[15] λ_D is the Debye length at the critical layer, and L is the scale length of the density gradient. Using the experimental conditions, i.e., $T_e=300$ eV, incident laser angle $\theta=50^\circ\pm18^\circ$, and $I=1.3\times10^{12}$ W/cm^2, Eq. (3) gives us the density depression $\delta N/N_0$ as a function of the scale length L. For a density depression larger than 10% L must be shorter than 200 μm, which is too short to form the 250-μm depressed region. Taking into account the plasma expansion velocity of $(1-2)\times10^7$ cm/sec and the velocity spread, the scale length L cannot be larger than 200 μm.

Therefore, in order to explain the observed frequency shift of 2.5×10^{10} Hz (80 Å), we cannot neglect the second term in Eq. (2). Density modulation has been observed to propagate in a plasma with the ion sound-wave velocity in microwave-plasma-interaction experiments.[16] Let us suppose that during the period of the increase of laser intensity the length of the depression channel D increases to produce a red-shift coinciding with the density depression. Using this effect as the contribution of the second term and assuming $\partial D/\partial t\simeq$ ion sound speed, typical values of $\delta N/N$ and D are found to be 70% and 80 μm. Similar results (60%–70% depression and 50 μm) are reported to have been observed in CO_2 laser plasma interaction experiments but with a long laser pulse.[17]

In a Nd-glass laser experiment, one of the authors reported[3] that a red-shifted spectrum was observed at the leading portion of the incident laser pulse and a blue-shifted spectrum at the tail. The introduction of the movement of the front of the density-depressed region can explain the observed results consistently. It is interesting to note that there is no blue side peak for the long-pulse case. This can be explained by the laser-pulse wave form which has a sharp rise of 1 nsec and gradual decay of 70 nsec. In this case no relaxation of the density depression can be expected. The modulational instability introduces the density depression in the cutoff region due to resonance absorption by linear conversion of the laser field. The density changes will be larger than estimated by Eq. (3) when the resonantly excited waves become unstable. This may lead to the formation of hot spots in the interaction region by laser-beam filamentation. These effects are important processes in the interaction at higher incident laser energy densities.

[1]C. Yamanaka, T. Yamanaka, T. Sasaki, K. Yoshida, M. Waki, and H. B. Kang, Phys. Rev. A 6, 2335 (1972).
[2]C. Yamanaka, T. Yamanaka, T. Sasaki, J. Mizui, and H. B. Kang, Phys. Rev. Lett. 32, 1038 (1974).
[3]C. Yamanaka, T. Yamanaka, J. Mizui, and M. Yamaguchi, Phys. Rev. A 11, 2138 (1975).
[4]C. Yamanaka, M. Yokoyama, S. Nakai, T. Sasaki, K. Yoshida, M. Matoba, C. Yamabe, T. Yamanaka, J. Mizui, N. Yamaguchi, and K. Nishikawa, IEEE/OSA Conference on Laser Engineering and Application,

Washington, D. C. 1975 (paper No. 11-7) (unpublished).
[5]S. Nakai, M. Matoba, S. Uda, H. Fujita, H. Toya, H. Nishimura, A. Nakamura, and C. Yamanaka, Rev. Laser Eng. 2, 35 (1975).
[6]M. Matoba, H. Nishimura, H. Toya, H. Fujita, K. Iba., S. Nakai, and C. Yamanaka, Tech. Rep. Osaka Univ. 26, 139 (1976).
[7]K. Itoh and S. Inoue, Phys. Rev. Lett. 37, 508 (1976).
[8]D. F. Dubois, in *Laser Interaction and Related Plasma Phenomena* edited by H. J. Schwarz and H. Hora (Plenum, New York, 1974), Vol. 3 A, p. 267.
[9]C. Yamabe, M. Yokoyama, and C. Yamanaka, Phys. Lett. A 50, 349 (1974).
[10]E. Fabre and C. Stenz, Phys. Rev. Lett. 32, 823 (1974).
[11]K. B. Mitchell, T. F. Stratton, and P. B. Weiss, Appl. Phys. Lett. 27, 11 (1975).
[12]J. J. Turechek and F. F. Chen, Phys. Rev. Lett. 36, 720 (1976).
[13]R. Massey, K. Berggren, and Z. A. Pietrzyk, Phys. Rev. Lett. 36, 963 (1976).
[14]K. G. Estabrook, E. J. Valeo, and W. L. Kruer, Phys. Fluids 18, 1151 (1975).
[15]V. L. Ginzburg, *The Properties of Electromagnetic Waves in Plasma* (Pergamon, New York, 1964).
[16]H. Ikeji, K. Nishikawa, and K. Mima, J. Phys. Soc. Jpn. 37, 766 (1974).
[17]T. P. Donaldson and I. J. Spalding, Phys. Rev. Lett. 36, 467 (1976).